

# 3D FULL PREDICTIVE THERMAL CHAIN FOR GAS TURBINE COMBUSTOR METAL TEMPERATURE

E. Mercier\*, L. Tessé\*\*, N. Savary\*\*\*  
 \*SNECMA, \*\*ONERA, \*\*\*TURBOMECA

**Keywords:** convective, radiative, effusion holes, combustor liners

## Abstract

During the last two decades, CFD tools have significantly been improved and take now part of the design process of turbomachinery components. Snecma, Turbomeca with the support of ONERA and the CERFACS have developed a 3D computational chain for combustor metal temperature forecast.

This chain is part of a life analysis process. Indeed, in order to achieve a pertinent life analysis of combustor liners, it is necessary to be able to foresee the most accurate 3D liner thermal map. The thermal gradients play indeed a crucial role in life analysis process.

That is why it has been necessary to develop this 3D chain.

This article describes the strong interaction existing between all the 3D codes (thermal, aerothermochemical, radiative) and proposes an iterative computational chain to take into account all the physical phenomena that take place in a combustor chamber.

## 1 Thermal description of the combustor

The main thermal exchanges that appear in a combustor are shown in Figure 1.

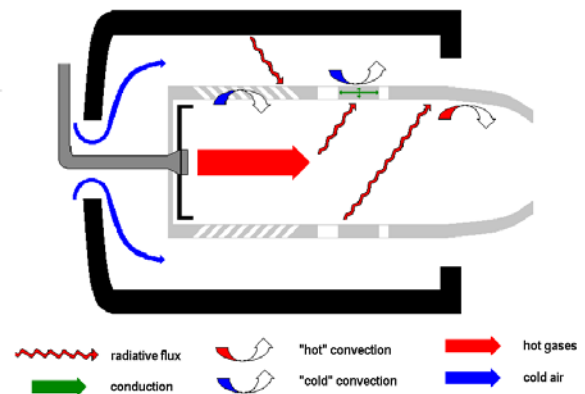


Fig. 1. Thermal fluxes.

The radiative flux due to the hot gases and the soot particles is the main hot flux. The convective flux can either cool the wall or warm it: it depends on the effectiveness of the cooling system.

The main cooling flux is the convective flux inside the effusion cooling holes.

The thermal fluxes on and inside the effusion cooled wall are represented in Figure 2.

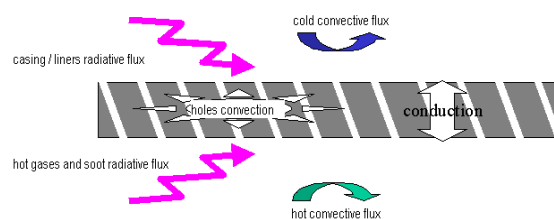


Fig. 2. Liner thermal fluxes.

In our methodology, the 3D CFD and radiative transfer calculations are performed on the whole domain inside the combustor liners. Thus they enable to extract the convective and radiative fluxes on the hot side of the liner walls.

In this methodology, the convective flux inside effusion cooling holes and the cold convective flux are evaluated thanks to correlations. The radiative flux exchanged between the liners and the casing is also taken into account considering an imposed casing temperature.

Smaller combustor sizes allow to perform 3D CFD and radiative calculations inside and around the combustor at the same time. The convective flux inside effusion cooling holes is the only heat flux evaluated thanks to correlations. This kind of calculations concern future evolution of the methodology.

## 2 Computational chain and iterative methodology

The 3D computational chain includes three different codes to take into account each physical phenomenon which influences the metal temperature. The first one is a turbulent, compressible, reactive 3D CFD code named N3S-Natur ([9], [10]) which enables to extract the convective variables on the liner walls. Furthermore, this code enables to predict the 3D soot field thanks to a model [8]. Using this preliminary calculation a radiative transfer code named ASTRE, developed by ONERA, computes the radiative flux on the hot side of the liner walls and the radiative power in the medium, which is the radiative source term in the energy balance equation solved in the CFD code. Then the commercial code (ABAQUS for Snecma or ANSYS for Turbomeca) is used to perform a calculation of the conduction inside the liner walls. For this computation, the convective and radiative fluxes on both sides of the walls and the cooling due to the convection inside the effusion holes, as shown in Figure 2, are taken into account.

In order to simulate the strong interactions existing between all these physical phenomena,

these three calculations have to be performed in an iterative process.

In this methodology, the radiative transfer code ASTRE and the conduction one ABAQUS or ANSYS converge automatically. To save computational time, only the CFD calculation can be partially converged during each global iteration of this process.

### 2.1 Coupling methodology

The strong interaction between all those codes can be easily understood if we consider the 0D formulations of the convective and radiative fluxes (Reeves formulation) used in 1D codes

$$\Phi_{conv} = h_{conv} \cdot (T_{conv} - T_{wall}) \quad (1)$$

$$\Phi_{rad} = \sigma \cdot C \cdot \epsilon_f \cdot (T_f^4 - \alpha_f / \epsilon_f \cdot T_{wall}^4) \quad (2)$$

Both fluxes depend on the wall temperature.

The influence of the wall temperature is not the only reason to couple these three codes. The radiative power computed by the radiative transfer code must also be taken into account in the energy balance equation solved in the CFD code

$$\frac{\partial \rho h_i}{\partial t} + \frac{\partial \rho h_i u_j}{\partial x_j} = \frac{\partial p}{\partial t} + \frac{\partial (u_i \tau_{i,j} + J_j^h)}{\partial x_j} + u_j F_j + P_{rad} \quad (3)$$

Thus the coupling methodology can be described as shown in Figure 3.

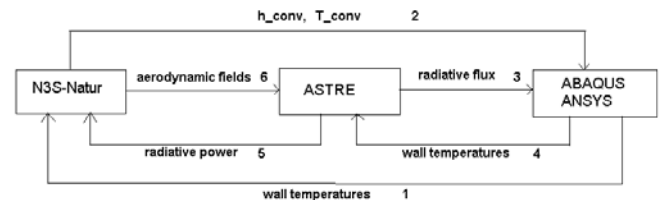


Fig. 3. Code coupling methodology.

Ways 2 and 3 correspond respectively to the effects of the convective and radiative fluxes on

the wall temperature calculated by the conduction code.

The equation (1) is solved thanks to the way 2 that leads to  $h_{conv}$  and  $T_{conv}$ , using wall law description for iteration numbers higher or equal to two (because  $T_{wall}$  imposed leads to  $\Phi_{conv} \neq 0$  and then  $h_{conv} \neq 0$ ) and a “differentiation” methodology for the first adiabatic iteration (because  $\Phi_{conv} = 0$  imposes  $h_{conv} = 0$ ). The radiative flux  $\Phi_{rad}$  absorbed by the wall is calculated in a 3D approach by the code ASTRE using a  $T_{wall}$  value thanks to the equation (9) (this equation replaced the equation (2) used in 1D codes).

Another slightly different approach can also be applied : this one has been used for the plate (see 3.2) . The radiative flux is linearised and expressed as a linear function of the wall temperature and the convection temperature. Thus, the boundary conditions of the conduction code can be written as in equation (5)

$$\Phi_{conv} = h_{conv} \cdot (T_{conv} - T_{wall}) \quad (1)$$

$$\Phi_{rad} = h_{rad} \cdot (T_{conv} - T_{wall}) \quad (4)$$

$$\Phi_{conv} + \Phi_{rad} = (h_{conv} + h_{rad}) \cdot (T_{conv} - T_{wall}) \quad (5)$$

This approach is used to improve convergence of the thermal chain. This approach is valid only in the scope of iterating the chain until convergence of the combustor wall temperatures.

Ways 1 and 4 correspond to the influence of the wall temperatures on the CFD and radiative transfer calculations. This imposes to use an iterative process to make these wall temperatures converge.

The way 5 enables to take into account the radiative power in the equation (3). To finish with, 3D temperature and species fields (way 6) are necessary to perform a 3D radiative transfer calculation.

## 2.2 Modelling

- *Convective variables extraction :*

The 3D CFD calculation gives access to the convective variables on the liner walls. N3S-Natur is an unstructured, turbulent, reactive, multi-species, compressible Navier-Stokes code, which enables to take into account on the same boundary condition effusion cooling entrance and wall laws. That point was first of all necessary to be able to realize such a coupling effect with a conduction code.

In our methodology, the **first CFD calculation** is supposed adiabatic

$$\Phi_{conv} = 0$$

$$\Rightarrow T_{conv} = T_{wall} \quad (6)$$

To be able to extract a convective coefficient, a “differentiation” methodology has been realized by performing another calculation and imposing  $T_{wall} = T_{conv} + 100^\circ\text{C}$ . Thus the equation (1) leads to

$$h_{conv} = \Phi_{conv} / 100 \quad (7)$$

For **other iterations**, the wall law description is used to extract the convective variables. Concerning a logarithm wall law

$$\Rightarrow \begin{cases} T_{conv} = T_{fluid\_first\_mesh} \\ h_{conv} = \frac{\rho_p c_p u_f}{T^+} \end{cases} \quad (8)$$

Another approach consists in starting the first iteration with “supposed“ wall temperatures and the formulation of equation (8). A study on a plate (see 3.2) has been realised to check that the result of the thermal chain was not dependant on initial wall temperatures.

This kind of description of the hot convective flux is used to optimize the thermal convergence. Indeed, imposing both radiative and convective fluxes would introduce numerical problems for the convergence of the thermal code ABAQUS or ANSYS. Indeed it has already been remarked that using both

fluxes imposes to relax the fluxes in order to converge.

- **Radiative flux and radiative transfer modelling :**

The second step of the computational chain consists in a radiative transfer calculation with the ASTRE code based on a Monte Carlo method [1,5-7]. The Forward Method (FM) is used in this study. This computation leads to new fields of radiative flux and power which are used in the next conduction and aerothermochemistry calculations respectively.

The radiative flux at a point  $P$  of a grey wall is given by

$$\Phi_{rad}(P) = \varepsilon_p \int_0^{+\infty} \int_{2\pi} I_\nu(P, \vec{u}) |\vec{u} \cdot \vec{n}| d\Omega d\nu - \varepsilon_p \sigma T_p^4, \quad (9)$$

and the radiative power at a point  $P$  of the medium writes

$$P_{rad}(P) = \int_0^{+\infty} \int_{4\pi} \kappa_\nu(P) I_\nu(P, \vec{u}) d\Omega d\nu - 4\pi \int_0^{+\infty} \kappa_\nu(P) I_\nu^o(T_p) d\nu, \quad (10)$$

where  $\varepsilon_p$  is the grey wall emissivity at the point  $P$ ,  $I_\nu(P, \vec{u})$  the incident directional spectral intensity at the point  $P$ ,  $\vec{u}$  the unit vector of the incident direction associated with the elementary solid angle  $d\Omega$ ,  $\vec{n}$  the unit vector normal to the wall at the point  $P$ ,  $\nu$  the wavenumber,  $\sigma$  the Stefan constant equal to  $5.67 \cdot 10^{-8} \text{ Wm}^{-2}\text{K}^{-4}$ ,  $T_p$  the temperature at the point  $P$ ,  $I_\nu^o(T_p)$  the spectral equilibrium intensity at temperature  $T_p$  and  $\kappa_\nu(P)$  the spectral absorption coefficient at the point  $P$  of the medium given by

$$\kappa_\nu(P) = \kappa_\nu^{gas}(P) + \kappa_\nu^{soot}(P). \quad (11)$$

The spectral absorption coefficient of the gas mixture  $\kappa_\nu^{gas}$  is given either by a High Pressure Box Model [2] or by a CK model [4] for applications at atmospheric pressure. The  $\text{CO}_2$  and  $\text{H}_2\text{O}$  parameters of the HPBM are derived from those of the statistical narrow band model of Soufiani and Taine [3]. The  $\text{CO}_2$  and

$\text{H}_2\text{O}$  parameters of the CK model are those generated by Soufiani and Taine [3]. From detailed discussion of Tessé [5], the spectral absorption coefficient (in  $\text{m}^{-1}$ ) of the soot particles, at a point  $P$  of the medium, is given by

$$\kappa_\nu^{soot}(P) = 550 \nu f_\nu(P), \quad (12)$$

where  $\nu$  is the wavenumber (in  $\text{cm}^{-1}$ ) and  $f_\nu$  the soot volume fraction. Radiation scattering by soot particle aggregates is not considered in the radiative transfer calculations.

- **Soot formation model:**

Snecma has integrated the LOS\_fv model developed [8] by the University of Lund (Sweden) in its 3D CFD reactive code N3S-Natur. This model developed during the European program CFD4C (Computational Fluid Dynamics For Combustion) takes into account the physico-chemical phenomena as the nucleation, the surface growth, the fragmentation and the oxidation.

The LOS\_fv model needs few N3S-Natur variables : the average values of pressure, temperature, dissipation rate scale, Zeldovitch variable and its variance. The soot formation calculation is performed on a converged aerothermochemical field. The LOS\_fv model CPU performance is due to the use of a library of flame calculated by using a detailed model of the n-C<sub>10</sub>H<sub>22</sub> mechanism and a complex soot model. The production terms are stored in flame library for different values of pressure, temperature, Zeldovitch variable and instantaneous scalar dissipation rate.

This soot model has been analysed by Snecma and compared with experimental data. The model leads to good spatial distribution of soot volume fraction inside the combustor, but the levels do not crosscheck the experimental measurements. Thus, thanks to Snecma experience, a factor has been included into the model to fit the levels to the experimental data.

### 3 Chosen configurations

#### 3.1 Geometric configurations

Two configurations have been calculated: an effusion cooled plate by Turbomeca and a combustor by Snecma.

The Snecma combustor calculated in this paper is the HP Core demonstrator DEM21 for civil turbomachinery.. It's a single annular combustor composed with 18 injectors. The metal liner thickness are protected with a thermal barrier. The liners are cooled with effusion cooling. The configuration used to check robustness, convergence and predictability of the thermal chain is an effusion cooled plate tested at TURBOMECA and for which temperature walls have been measured with infrared thermometry.

#### 3.2 Cross-checking point

The DEM21 studied point is the Red Line point. Indeed this point is the hottest one of the rig test campaign realized on the banc K11 of the CEPR:

Diffuser exit conditions :

$$T_{31} = 854K$$

$$P_{T31} = 30 \text{ bars}$$

Combustor chamber exit :

$$FAR_{40} = Q_{fuel}/Q_{air} = 34\%$$

$$Q_{36} = 34 \text{ kg/s}$$

On this point, experimental exit combustor temperature profile has been measured and thermocouples on the cold side of the liner walls have also been used to evaluate the metal temperature. The trouble with thermocouples is that they are not able to give a pertinent 2D vision of temperature gradients. For example, in high gradient zones the thermocouple dispersion can be important. Furthermore, to be able to describe an average injector, there should be 18

thermocouples for each position, which is not the case.

For convergence and predictability calculations, the aerodynamic conditions chosen correspond to the maximum of radiative and convective fluxes on the Turbomeca plate:

Cold side conditions :

$$T_{31} = 330K, P_{T31} = 1 \text{ bar}$$

Hot side conditions :

$$T_{41} = 1400K, P_{T41}-P_{T31} = 0.05 \text{ bar}$$

### 4 Results

#### 4.1 Multiperforated plate calculations

##### 4.1.1 Robustness and convergence checking

The convergence of the thermal chain has been realized with the approach of initial wall temperature conditions and radiative flux extraction. Indeed, if convergence is demonstrated with this approach, the "differentiation" methodology could be abandoned.

The study consisted in running two sets of iteration with the same boundary conditions and the same coupling methods. The only difference was the initial wall temperature used for the first convective and radiative calculations.

The first run (blue lines in Figure 4) used a 500K uniform temperature on the plate which is everywhere below the measured temperature.

The second run (red lines in Figure 4) used a 1000K uniform temperature on the plate which is everywhere above the measured temperature.

In order to check the convergence of the thermal chain, the mean node absolute value of temperature variation between two iterations was monitored.

Six iterations have been performed for the 500K initial temperature run and the convergence

criteria reached 3K which is good enough considering the required precision (about 10K). Seven iterations have been performed for the 1000K initial temperature run but in this case, the convergence criteria did not go under 6K. This is visible in Figure 4: the temperature profile corresponding to the last iteration is not very smooth and some more iterations could lead to better quality results. This can be easily explained by the fact that the 1000K initial profile was farther from the final solution than the 500K initial profile, resulting in more iterations needed to converge with the same quality level.

Nevertheless, Figure 4 allows us to conclude that both sets of calculations converge to the same result which demonstrates the independency and robustness of the result into a very large range of initial wall temperature conditions.

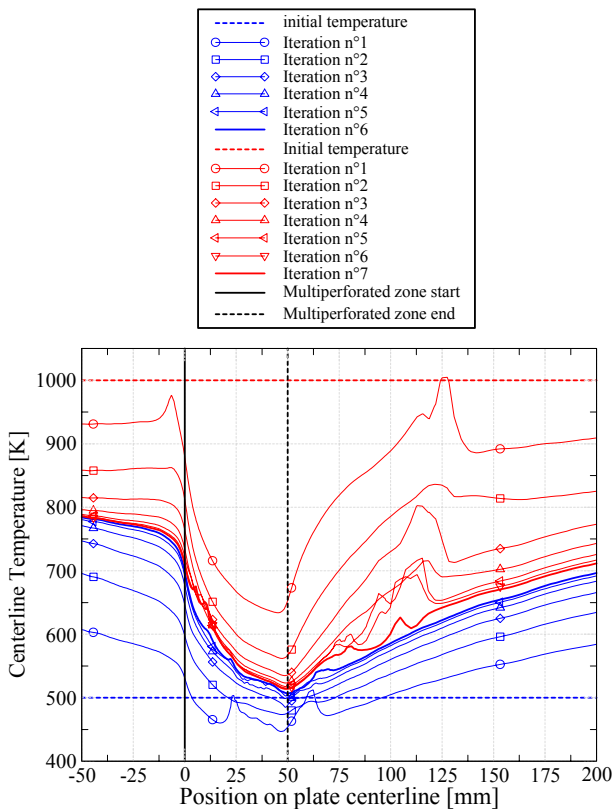


Fig. 4. Evolution of temperature profiles along the plate during iterative process.

#### 4.1.2 Predictability of the thermal chain

The iterative process between convective, radiative and conductive calculations has been validated comparing the results to measurements.

The available measurements correspond to wall temperatures acquired by infrared thermometry. Temperatures along the middle line of the plate are presented in order not to be influenced by side effects.

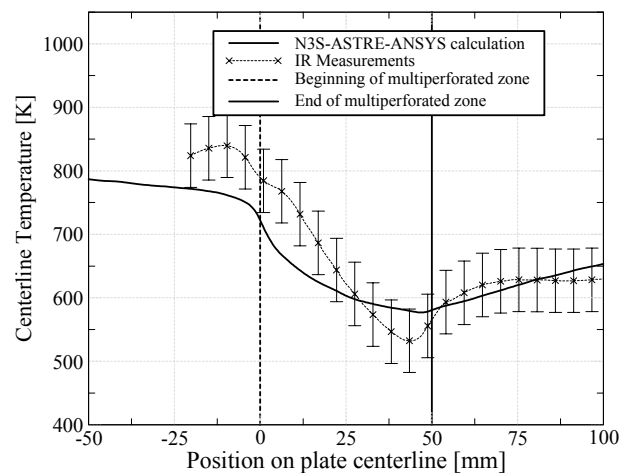


Fig. 5. Comparison between N3S-ASTRE-ANSYS calculation and Infrared thermometry measurements.

Fluxes were not measured and thus could not be compared to calculations.

Calculated and measured wall temperatures are presented in Figure 5. The global temperature levels and evolutions are well represented by calculations. Nevertheless, some differences going up to 100K are visible, especially in the multiperforated zone. This can be explained by two factors :

- the measurements uncertainties evaluated by thermocouple – IR thermometry comparisons and repeatability is relatively high and can explain part of the 100K
- the 1D model used in order to predict convection and air heating into effusion holes may be too simple.

Some improvements in aerodynamic and thermal modelling of multiperforated zones might give better results.

## 4.2 DEM21 combustor calculations

Three kinds of calculations have been realized to access to the exit combustor and liner wall temperature maps:

1. 3D CFD calculation: N3S-Natur
2. 3D radiative transfer calculation: ASTRE
3. 3D thermal calculation: ABAQUS

The methodology consists in converging the CFD calculation for each iteration. That means that we realized a weak coupling between all those codes.

In the following result presentation, all the variables are extracted along the injector axis on the outer liner, as shown in Figure 6.

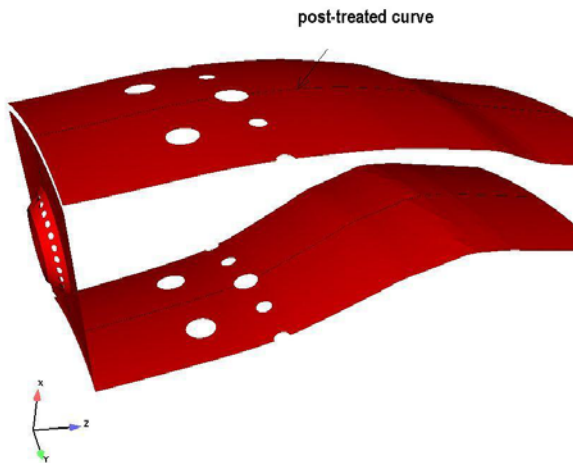


Fig. 6. Injector axis on the outer liner.

### 4.2.1 CFD calculations

As described before, the first 3D CFD calculation is supposed adiabatic. This first converged calculation has the greatest CPU cost. Other iterations, taking into account the wall temperature and radiative power fields given by the previous ASTRE and ABAQUS calculations, are performed starting from this first calculation.

These calculations allow us to check the evolutions of the exit combustor temperature profile, of the convective variables on the hot side wall and of the soot distribution.

#### 4.2.1.1 Thermal boundary condition extraction

The convective variables, after 4 iterations, are plotted in Figures 7 and 8.

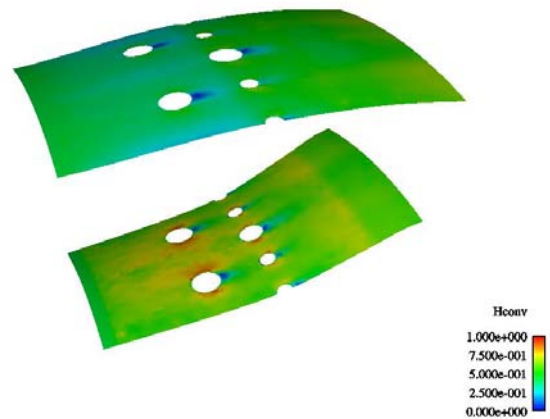


Fig. 7. Dimensionless convective coefficient field.

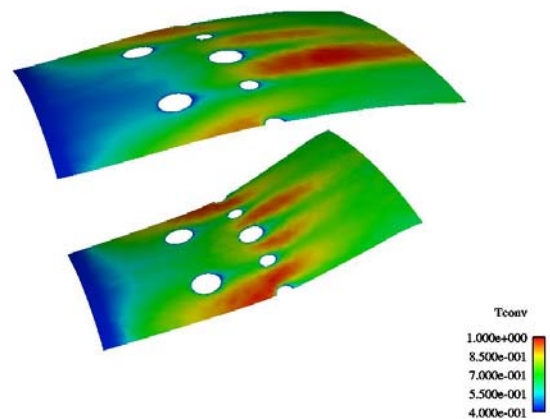


Fig. 8. Dimensionless convective temperature field.

The film cooling effect at the beginning of the liners is shown in Figure 8. We can also see the interaction between hole jets and the principal hot airflow on the convective variables. Indeed, the hot airflow velocity increases between dilution holes. On the contrary, downstream the holes the convective exchanges decrease.

The evolutions, along the injector axis, of the convective variables on the hot side of the outer liner are shown in Figures 9 and 10 for each iteration.

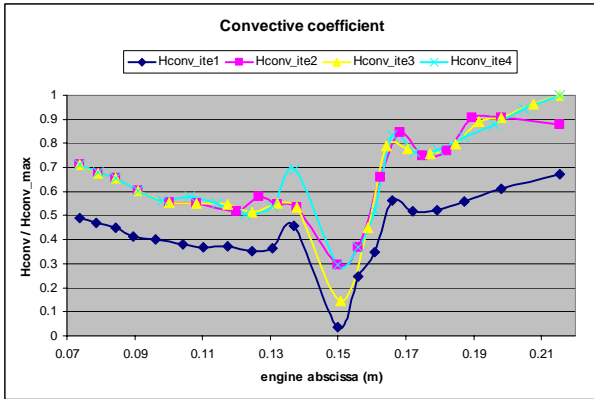


Fig. 9. Evolution, along the injector axis, of the dimensionless convective coefficient on the hot side of the outer liner.

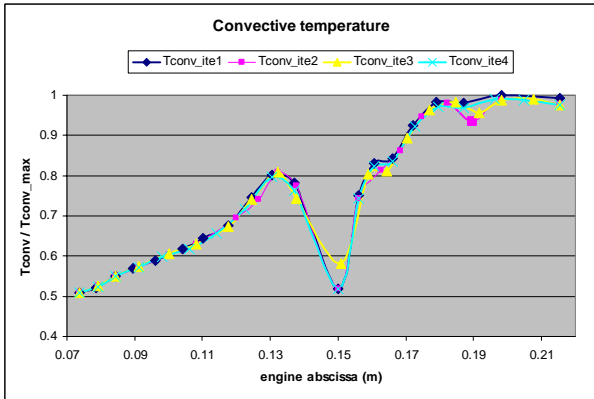


Fig. 10. Evolution, along the injector axis, of the dimensionless convective temperature on the hot side of the outer liner.

The convective variables seem to converge after the third iteration, except just near the big dilution holes where the convective coefficient still seems to evolve.

#### 4.2.1.2 Soot and temperature results

- **Soot results**

The soot 3D distribution is not really affected by the coupling of all those codes because the radiative heat loss remains small compared to the combustion heat release. The converged distribution is plotted in Figure 11.

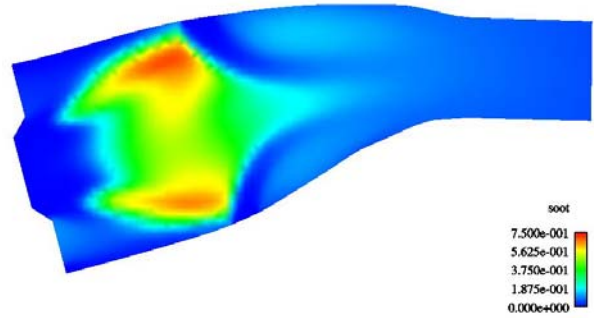


Fig. 11. Dimensionless soot concentration field in the injector plane

The iterations do not really influence the soot concentration. Indeed the 3D field and the level of soot concentration do not really change between the first and the fourth iteration.

- **Exit temperature profile**

As for the soot distribution, the exit temperature profile is not really influenced by the wall temperature and the radiative power. Indeed, the temperature profile does not evolve after the second iteration, as shown in Figure 12.

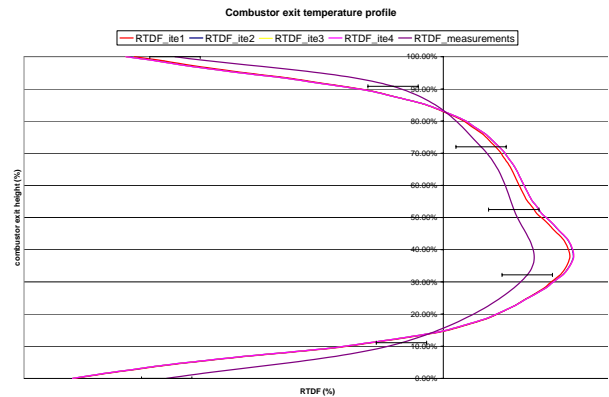


Fig. 12. RTDF profile.

$$RTDF(r) = \frac{\langle T_{40}(r) \rangle - \langle T_{40} \rangle}{\langle T_{40} \rangle - \langle T_{31} \rangle} \quad (14)$$

Plane 40 : combustor exit

Plane 31 : diffuser exit

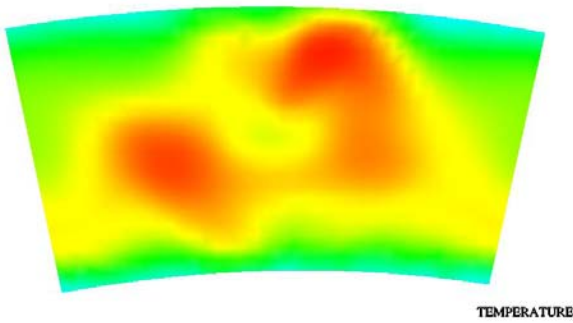


Fig. 13. 2D exit combustor temperature map.

### 4.2.2 Radiative transfer calculations

Using the temperature, the soot and species concentration 3D distributions given by the previous N3S-Natur calculation, but also the 2D wall temperature field obtained from the previous ABAQUS calculation and the wall grey emissivity specified by the user, the 3D radiative code ASTRE computes the 3D field of radiative power inside the combustor and the 2D distribution of wall radiative flux on the hot side of the liners. These two radiative quantities are integrated over the whole spectrum. The 2D distribution of the radiative flux ( $W/m^2$ ), after the fourth iteration, is plotted in Figure 14.

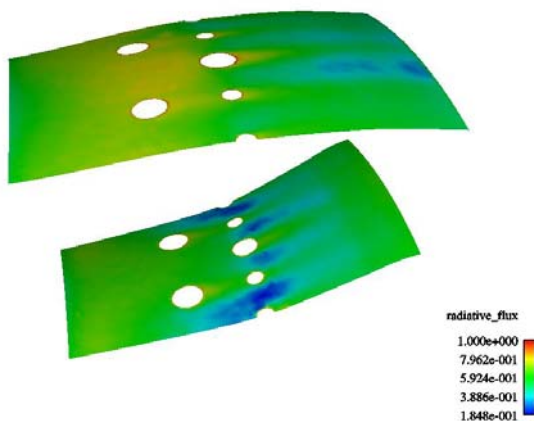


Fig. 14. Dimensionless wall radiative flux field ( $W/m^2$ ).

The evolution of the average radiative flux on the outer and inner liners, is given in Table 1.

Average value	ite 1	ite 2	ite 3	ite 4
$\Phi_{rad}(kW/m^2)$	<b>1</b>	<b>0.79</b>	<b>1.05</b>	<b>1.05</b>
$\Phi_{rad} / \Phi_{rad\_ite1}$				

Table 1. Convergence of the average radiative flux.

The radiative flux seems to converge after the third iteration.

The evolution, along the injector axis, of the radiative flux on the hot side of the outer liner is given for each iteration in Figure 15.

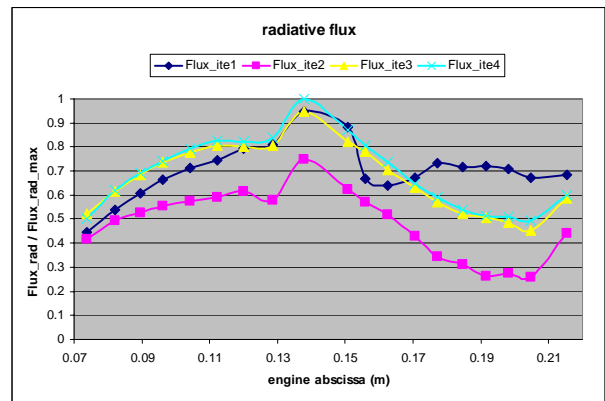


Fig. 15. Evolution, along the injector axis, of the dimensionless radiative flux on the hot side of the outer liner.

This figure confirms that the radiative flux converges after the third iteration.

### 4.2.3 Thermal calculations

As seen before, the main hot side thermal boundary conditions converge after 4 iterations. Taking into account, for each iteration, the same convective coefficient and temperature inside the effusion cooling holes and on the cold side wall, the thermal calculation must also converge at the fourth iteration.

The converged metal temperature field is plotted in Figure 16.

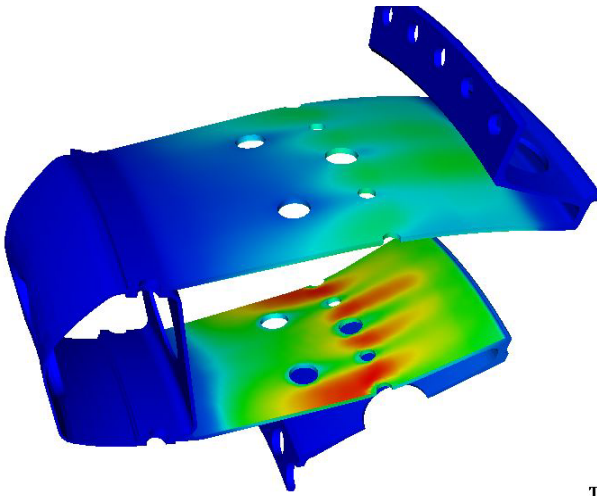


Fig. 16. Metal temperature field (K).

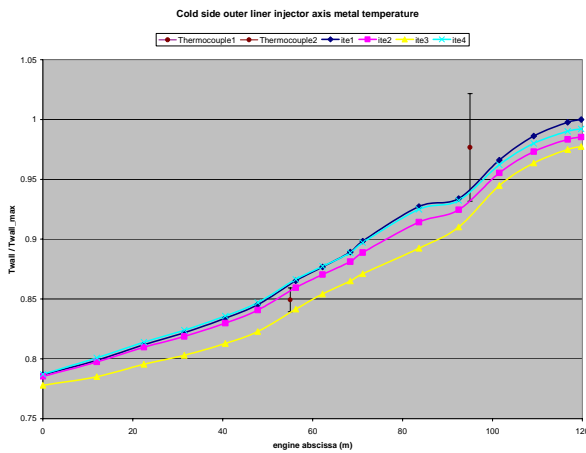
Table 2. Convergence of the wall temperature on the hot side of the outer liner.

The maximum metal temperature seems also to converge, as shown in Table 3. There is a remarked before a great decrease of the maximum metal temperature between the first and second iteration.

Maximum metal temperature	Ite 1	Ite 2	Ite 3	Ite 4
$T_{max} (K)/T_{max\_ite1}$	<b>1</b>	<b>0.95</b>	<b>0.946</b>	<b>0.959</b>

Table 3. Convergence of the maximum metal temperature.

The evolution, along the injector axis, of the metal temperature on the cold side of the outer



liner is given in Figure 17 for each iteration.

Fig. 17. Evolution, along the injector axis, of the metal temperature on the cold side of the outer liner.

The experimental uncertainty is represented by vertical segments in Figure 17.

The injector axis does not really show the evolution of the hottest area. The wall temperature evolution on the hot side of the outer liner is summarized in Table 2. We can remark that the metal temperature decreases a lot between the first and second iteration.

Temperature variation	ite2 – ite1	ite3 – ite2	ite4 – ite3
Max $\Delta$	210	66	26
Min $\Delta$	0	0	0
Average $\Delta$	44	26	12

As shown by Turbomeca, it should also be a solution to initialize the first iteration with an average value of the hot side liners wall temperature. It would enable to avoid the “differentiation” methodology and then one 3D CFD calculation.

## 5 Conclusion

This study demonstrates the capability of 3D numerical simulation codes to handle the 3 main heat fluxes for combustor wall temperature prediction. It demonstrates in particular the robustness and convergence of the methodology as well as its applicability to real combustor geometry.

## 6 Future evolutions

1. Use a better soot model,
2. Perform a better multiperforated plate model
3. Evaluate the critic coupling ways in order to optimize the coupling,
4. Compare with strong coupling,
5. Automate the iterative chain.

## References

- [1] Dupoirieux F, Tessé L, Avila S and Taine J. An optimized reciprocity Monte Carlo method for the calculation of radiative transfer in media of various optical thicknesses. *Int. J. Heat Mass Transfer*, Vol. 49, pp 1310-1319, 2006.

- [2] Pierrot L. Développement, étude critique et validation de modèles de propriétés radiatives infrarouges de CO<sub>2</sub> et H<sub>2</sub>O à haute température. Application au calcul des transferts dans des chambres aéronautiques et à la télédétection Thèse de Doctorat n°1997-17, Ecole Centrale Paris, France, 1997.
- [3] Soufiani A and Taine J. High temperature gas radiative property parameters of statistical narrow-band model for H<sub>2</sub>O, CO<sub>2</sub> and CO, and correlated-k model for H<sub>2</sub>O and CO<sub>2</sub>. *Int. J. Heat Mass Transfer*, Vol. 40, pp 987-991, 1997.
- [4] Taine J and Soufiani A. Gas IR radiative properties: from spectroscopic data to approximate models. *Advances in Heat Transfer*, Vol. 33, pp 295-414, 1999.
- [5] Tessé L. Modélisation des transferts radiatifs dans les flammes turbulentes par une méthode de Monte Carlo. Thèse de Doctorat n°2001-34, Ecole Centrale Paris, France, 2001.
- [6] Tessé L, Dupoirieux F, Zamuner B and Taine J. Radiative transfer in real gases using reciprocal and forward Monte Carlo methods and a correlated-k approach. *Int. J. Heat Mass Transfer*, Vol. 45, pp 2797-2814, 2002.
- [7] Tessé L, Dupoirieux F, and Taine J. Monte Carlo modelling of radiative transfer in a turbulent sooty flame. *Int. J. Heat Mass Transfer*, Vol. 47, pp 555-572, 2004.
- [8] Dederichs A, Bathasar M and Mauss F Introduction of heat loss terms in flamelet library, CFD4C D4.6, 2001
- [9] Brun G (1988) Développement et application d'une méthode d'éléments finis pour le calcul des écoulements turbulents fortement chauffés, Thèse , Ecole Centrale de Lyon, 1988.
- [10] Ravet F, Baudoin C and Schultz JL Modélisation numérique des écoulements réactifs dans les foyers de turboréacteurs, Rev Gén Therm, 1997